A recurrent KCNQ2 pore mutation causing early onset epileptic encephalopathy has a moderate effect on M current but alters subcellular localization of Kv7 channels

Affef Abidi, Jérôme Devaux, Florence Molinari, Gisèle Alcaraz,
François-Xavier Michon, Julie Sutera-Sardo, Hélène Becq, Caroline Lacoste,
Cécilia Altuzarra, Alexandra Afenjar, et al.

A recurrent *KCNQ2* pore mutation causing early onset epileptic encephalopathy has a moderate effect on M current but alters localization of Kv7 channels

Affef Abidi [a,b], Jérôme J. Devaux [c], Florence Molinari [d,e], Gisèle Alcaraz [a,b], François-Xavier Michon [d,e],
Julie Sutera-Sardo [a,b,f], Hélène Becq [d,e], Caroline Lacoste [a,b,bb], Cécilia Altuzarra [g], Alexandra Afenjar [i,ii],
Cyril Mignot [h,i], Diane Doummar [ii], Bertrand Isidor [j], Sylvie N. Guyen [k], Estelle Colin [l], Sabine De La Vaissière [m],
Damien Haye [n], Adeline Trauffler [o], Catherine Badens [a,b,bb], Fabienne Prieur [p], Gaetan Lesca [q], Laurent Villard [a,b],
Mathieu Milh [a,b,f,*], Laurent Aniksztejn [d,e,**]

[a] *Aix-Marseille Université, GMGF, Marseille, France*
[b] *INSERM, UMR_S 910, Marseille, France*
[bb] *APHM, Hôpital d'enfants de la Timone, Département de génétique médicale et de biologie cellulaire, Marseille France*
[c] *Aix-Marseille Université, CNRS, CRN2M-UMR7286, Marseille, France*
[d] *Aix-Marseille Université, Institut de Neurobiologie de la Méditerranée (INMED), Marseille, France*
[e] *INSERM, UMR_S 901, Marseille, France*
[f] *APHM, Hôpital d'Enfants de la Timone, Service de neurologie pédiatrique, Marseille, France*
[g] *CHU Besançon, Service de génétique et neuropédiatrie, Besançon, France*
[h] *APHP, Service de Génétique Médicale et Centre de Références « Déficiences Intellectuelles de Causes Rares », Groupe Hospitalier Pitié-Salpêtrière, Paris, France*
[i] *Université Pierre et Marie Curie, Groupe de Recherche Clinique « Déficiences Intellectuelles de Causes Rares », Paris, France*
[ii] *APHP, service de neurologie pédiatrique, Hôpital Trousseau, Paris, France*
[j] *CHU de Nantes, Service de génétique médicale, Nantes, France*
[k] *CHU d'Angers, Service de neurologie pédiatrique, Angers, France*
[l] *CHU d'Angers, Département de Biochimie et Génétique, Angers, France*
[m] *CHU de Tours, Service de neurologie pédiatrique, Tours, France*
[n] *CHU de Tours, Service de génétique, Tours, France*
[o] *CHU de Lille, Service de neurologie pédiatrique, Lille, France*
[p] *CHU de Saint Etienne, Service de génétique médicale, France*
[q] *Hospices Civils de Lyon, Service de génétique, Lyon, France*

ABSTRACT

Mutations in the *KCNQ2* gene encoding the voltage-dependent potassium M channel Kv7.2 subunit cause either benign epilepsy or early onset epileptic encephalopathy (EOEE). It has been proposed that the disease severity rests on the inhibitory impact of mutations on M current density. Here, we have analyzed the phenotype of 7 patients carrying the p.A294V mutation located on the S6 segment of the Kv7.2 pore domain (Kv7.2^{A294V}). We investigated the functional and subcellular consequences of this mutation and compared it to another mutation (Kv7.2^{A294G}) associated with a benign epilepsy and affecting the same residue. We report that all the patients carrying the p.A294V mutation presented the clinical and EEG characteristics of EOEE. In CHO cells, the total expression of Kv7.2^{A294V} alone, assessed by western blotting, was only 20% compared to wild-type. No measurable current was recorded in CHO cells expressing Kv7.2^{A294V} channel alone. Although the total Kv7.2^{A294V} expression was rescued to wild-type levels in cells co-expressing the Kv7.3 subunit, the global current density was still reduced by 83% compared to wild-type heteromeric channel. In a configuration mimicking the patients' heterozygous genotype i.e., Kv7.2^{A294V}/Kv7.2/Kv7.3, the global current density was reduced by 30%. In contrast to Kv7.2^{A294V}, the current density of homomeric Kv7.2^{A294G} was not significantly changed compared to wild-type Kv7.2. However, the current density of Kv7.2^{A294G}/Kv7.2/Kv7.3 and Kv7.2^{A294G}/Kv7.3 channels were reduced by 30% and 50% respectively, compared to wild-type Kv7.2/Kv7.3. In neurons, the p.A294V mutation induced a mislocalization of heteromeric mutant channels to the somato-dendritic compartment, while the p.A294G muta-tion did not affect the localization of the heteromeric channels to the axon initial segment. We conclude that this

position is a hotspot of mutation that can give rise to a severe or a benign epilepsy. The p.A294V mutation does not exert a dominant-negative effect on wild-type subunits but alters the preferential axonal targeting of heteromeric Kv7 channels. Our data suggest that the disease severity is not necessarily a consequence of a strong inhibition of M current and that additional mechanisms such as abnormal subcellular distribution of Kv7 channels could be determinant.

Introduction

Kv7.2-5/*KCNQ2–5* channels are slow activating and non-inactivating voltage-gated potassium channels expressed in several neuronal populations (Jentsch, 2000; Brown and Passmore, 2009). Each subunit consists of intracellular N and C terminal domains and 6 transmembrane segments forming a voltage-sensing (S1–S4) and a pore (S5–P–S6) domains. Functional channels are formed by the homomeric or heteromeric assemblies of 4 subunits including Kv7.2 and Kv7.3, the two principal subunits underlying M current in many neurons (Wang et al., 1998; Battefeld et al., 2014; but see also Soh et al., 2014). Recent reports indicate that Kv7.2/Kv7.3 channels are selectively localized at the axonal initial segments (AIS) and at nodes of Ranvier in central and peripheral nervous systems where they are co-clustered with Nav channels (Devaux et al., 2004; Pan et al., 2006; Rasmussen et al., 2007; Battefeld et al., 2014). At these positions, Kv7 channels play a crucial role in controlling neuronal excitability (Yue and Yaari, 2006; Hu et al., 2007; Shah et al., 2008; Battefeld et al., 2014; Soh et al., 2014).

Previously, mutations in *KCNQ2* have only been reported in benign familial neonatal seizures (BFNS) (Biervert et al., 1998; Singh et al., 1998; Charlier et al., 1998). More recently, *de novo* mutations in *KCNQ2* were described in a severe form of neonatal epilepsy (early onset epileptic encephalopathy, EOEE), characterized by an early neonatal onset (first week) of stormy motor seizures, without any structural abnormality (but see Dalen Meurs-van der Schoor et al., 2014) and with variable outcome (Weckhuysen et al., 2012; Kato et al., 2013; Milh et al., 2013; Allen et al., 2014). Indeed, despite relatively similar early clinical features, the prognosis of *KCNQ2*-related epilepsies is highly variable. To date, there appears to be a broad separation between mutations of *KCNQ2* causing severe versus benign epilepsies but exceptions do exist (Borgatti et al., 2004; Steinlein et al., 2007). It was therefore proposed that the clinical variability of the *KCNQ2*-related epilepsy could be related to the functional consequence of mutations on M current and could thus be predictive of the neurological prognosis, a notion that was recently supported by two different studies (Miceli et al., 2013; Orhan et al., 2014).

Here, we investigated the early electro-clinical features and clinical evolution of 7 patients carrying a Kv7.2-p.A294V (Kv7.2[A294V]) mutation located within the S6 pore domain and compared the functional consequences of this mutation to an inherited mutation associated with BFNS (Kv7.2[A294G], Steinlein et al., 2007). In those patients, the p.A294V mutation was always associated with severe forms of neonatal epilepsy. Both mutations had the same functional impact on M current, and modestly reduced the global current density by ~30% as measured in Chinese hamster ovary cells (CHO) in the configuration mimicking the situation found in patients. However, the p.A294V but not the p.A294G mutation induced a redistribution of Kv7 channels to the somato-dendritic compartment of neurons. Thus, our data indicate that the severity of the disease is not necessarily associated with strong inhibition of M current and we postulate that additional mechanisms such as abnormal subcellular distribution of Kv7 channels could be determinant.

Patients and methods

Patients

KCNQ2 screening was performed for diagnosis purpose at the "Département de Génétique Médicale" of the Timone Children's Hospital in Marseille and in the Hôpital Femme-Mère-Enfant in Lyon. We received a total of 237 patient's DNA having an early onset epileptic encephalopathy (EOEE, n = 208) or benign familial neonatal seizures (BFNS, n = 29). We found *KCNQ2* mutations in 46 patients; 23 presenting EOEE (see Fig. 1) and 23 presenting BFNS. Some of the EOEE and BFNS-related mutations have already been published (Milh et al., 2013; Soldovieri et al., 2014). We found 7 patients (5 in Marseille and 2 in Lyon) carrying the same mutation in the *KCNQ2* gene, c.881C>T/p.A294V (NM_172107.2), and presenting an EOEE (see the
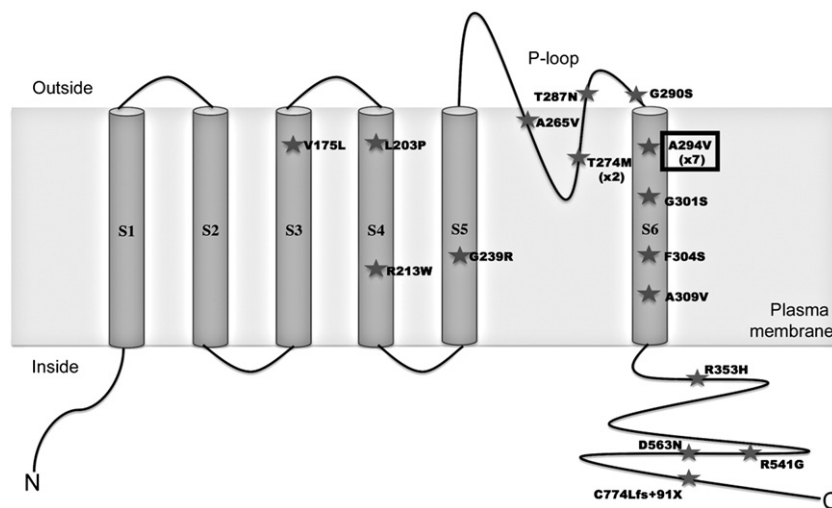

Fig. 1. Schematic presentation of the Kv7.2 subunit with the location of the different mutations associated with EOEE identified at the Timone Hospital in Marseille and in the Hôpital Femme-Mère-Enfant in Lyon. We analyzed the functional consequences and subcellular distribution of the Kv7.2 channel carrying the pore p.A294V mutation identified in 7 patients of our cohort.

Results section). The mutation p.A294V was never observed in the BFNS patient's DNA. All blood samples were obtained after receiving informed consent.

The pediatric neurologist ensuring the patients follow-up and the coordinator of the clinical study examined the phenotype of each patient, studied the retrospective clinical history and performed additional neurological examination. We paid a specific attention to epileptic seizures, MRI, development, evolution of head growth, age at seizure onset, type of seizure, electroencephalographic (EEG) aspects (suppression-burst, polymorph partial seizure), and antiepileptic drug response. This study was approved by local ethical committee (CPP Sud Mediterranée).

Molecular biology

Human cDNAs encoding Kv7.2 (# NM_172108.3) and Kv7.3 (# NM_004519.3) were subcloned into pcDNA3. We introduced the c.881C>T/p.Ala294Val and c.881C>G/p.Ala294Gly mutation (according to NM_172107.2) using the QuikChange II Site-Directed Mutagenesis Kit (Agilent) and verified the presence of the mutation using Sanger sequencing.

The hKv7.2-V5, hKv7.2^{A294V}-V5 and hKv7.2^{A294G}-V5 plasmids were constructed using standard PCR techniques and subsequently cloned into the pcDNA3.1/V5-His-TOPO vector for expression in mammalian cells. The V5 tag was inserted at the C-terminus of Kv7.2 without linker as previously described (Wen and Levitan, 2002).

Antibodies

A 21 amino acid peptide sequence (AGDEERKVGLAPGDVEQVTLA), corresponding to amino acids 36–57 from the N-terminal region of KCNQ3 was synthesized (Pan et al., 2006), conjugated to keyhole limpet hemocyanin, and two rabbits were immunized. The antisera were collected and purified against the peptide immunogen (Eurogentec, Seraing, Belgium). These antisera stained cells that were transfected with a cDNA encoding Kv7.3 but not Kv7.2 (data not shown). The rabbit antiserum against Kv7.2 was previously characterized (Lonigro and Devaux, 2009).

Cell culture and transfections

Chinese hamster ovary (CHO) cells were cultured at 37 °C in a humidified atmosphere with 5% CO_2 with a Gibco® F-12 Nutrient Mixture (Life Technologies) supplemented with 10% FBS (Fetal Bovine Serum) and 100 units/mL antibiotics/antimycotics (Life Technologies).

These cells were transfected using the Neon® Transfection System (Life Technologies) according to the manufacturer's protocol. Briefly, 100 000 cells in suspension were transfected with a total amount of 1 μg of DNA containing a reporter plasmid with the RFP gene (1:5) and cDNA constructs as followed: Kv7.2 (1); Kv7.2^{A294V} (1); Kv7.3 (1); Kv7.2 + Kv7.2^{A294V} (1:1); Kv7.2 + Kv7.3 (1:1); Kv7.3 + Kv7.2^{A294V} (1:1); Kv7.2 + Kv7.2^{A294V} + Kv7.3 (1:1:2); Kv7.2^{A294G} (1); Kv7.2 + Kv7.2^{A294G} (1:1); Kv7.3 + Kv7.2^{A294G} (1:1);

Table 1
Clinical features of patients carrying the Kv7.2-p.A294V mutation.

	HC at birth (cm)	Seizure onset (days)	Initial seizure type	Mode of beginning	Seizure offset: yes/no (age, treatment)	EEG: first week	Development at last evaluation (age of evaluation)
Patient 1	35	3	Tonic asymmetric: left or right head deviation, tonic extension of the four limbs	Stormy	Yes: 2 m, PHT	Suppression-burst until 3rd week. 3 weeks to 2 m: continuous traces, bilateral frontal and temporal spikes. >2 m: progressive decrease in spikes frequency. Normal sleep organization.	Unable to sit. Poor communication (1 y).
Patient 2 (Milh et al., 2013, patient 6)	34.5	2	Left and right clonic jerks, facial cyanosis	Subtile	Yes: 3 m, ND	Suppression-burst.	Poor head control, unable to sit, no voluntary movement, no language (2 y).
Patient 3 (Milh et al., 2013, patient 7)	36	1	Tonic contractions of one or several limbs, cyanosis	Stormy	No: 7 m, epileptic spasms 2–9 y, seizure free >9 y, monthly GTC seizures	Suppression-burst.	Establishes eye contact. Strabismus. Unable to sit, no speech (11 y).
Patient 4 (Milh et al., 2013, patient 15)	29 (30 weeks GA at birth)	8	Myoclonic jerks, multiple seizures daily	Stormy	Yes: 3 m, VPA	Suppression-burst.	Unable to sit. Unable to walk. Uses a few words (2–3 words). Understands simple orders. Strabismus, nystagmus (3 y).
Patient 5	35	1	Prolonged dystonic posture (opistotonos), then tonic asymmetric seizures. Paucisymptomatic seizures (EEG recordings only)	Stormy	Unknown, death at 6 weeks	Discontinuous, then suppression-burst until death.	NA
Patient 6	37	1	Tonic asymmetric and tonic–clonic	Stormy	Yes: 3 weeks, VPA	Slow background activity. Bilateral paroxysmal discharges. One tonic seizure.	Walk with aid. No language (16 m).
Patient 7	37	3	Tonic seizures	Stormy	Yes: 4 m, TPM + LVT	Suppression-burst. Bilateral paroxysmal discharges predominantly in the right fronto-temporal region.	Severe global delay harmonious. Unable to sit. Poor hand use (16 m).

EEG: electro-encephalogram; GA: gestational age; GTC: generalized tonic–clonic seizures; HC: head circumference; LVT: levetiracetam; m: months; NA: not available; ND: not determined; PHT: phenytoin; TPM: topiramate; VPA: valproic acid; y: year.

Table 2
Major clinical features in patients with the p.A294V mutation.

Normal HC at birth	7/7
Seizure onset before day 4	6/7
Predominant initial seizure type: tonic asymmetric	5/7
Initial EEG: suppression-burst	6/7
Seizure withdrawal before 6 months	5/7 (1 death)
Developmental delay	7/7
Walk with aid	1/7
Normal HC at the end of the follow up	7/7

EEG: electro-encephalogram; HC: head circumference.

and Kv7.2 + Kv7.2^{A294G} + Kv7.3 (1:1:2). Electroporation configuration was: 1400 V, 1 pulse, 20 ms. Following electroporation, cells were cultured on pre-coated glass coverslips and maintained at 37 °C and 5% CO$_2$ with a complete medium for 2 days before recordings.

Electrophysiology

The electrophysiological analysis of each of the p.A294V and p.A294G mutant channels was performed on the same day than the analysis of the wild-type control channels (Kv7.2 and Kv7.2 + Kv7.3) with the same batch of CHO cells. Cells were perfused at 1–2 ml/min with a solution of the following composition (in mM): 135 NaCl, 3.5 KCl, 5 NaHCO$_3$, 0.5 NaH$_2$PO$_4$, 1 MgCl$_2$, 1.5 CaCl$_2$, 10 HEPES, 10 glucose, and pH 7.3 adjusted with NaOH. Whole-cell patch-clamp recordings were performed with microelectrodes (borosilicate glass capillaries GC 150F-15, Harvard apparatus) filled with a solution containing (in mM): 135 KCl, 0.1 CaCl$_2$, 1.1 EGTA, 10 HEPES, 3 Mg^{2+}ATP, 0.3 Na$^+$GTP, 4 phosphocreatinine, pH 7.3 adjusted with KOH and a resistance of 4–6 MΩ. Data were sampled at 10 kHz and filtered with a cut-off frequency of 3 kHz using an EPC-9 amplifier (HEKA Electronik). Cell capacitance was determined with the whole cell capacitance compensation circuit of the EPC-9 amplifier. Overall, the mean value was 31.6 ± 1.72 pF (n = 242 cells). Voltage steps of 10 mV increment during 2 s from holding potential of −85 mV (or −105 mV in retigabine experiments) and up to +45 mV followed by a pulse to −65 mV for 1 s were applied to the cells in order to analyze the conductance–voltage (G–V) relationships and the kinetics of activation and deactivation of the channels. G values were obtained from peak amplitudes of the slow outward current divided by the driving force for K$^+$ ions with E$_K$ ~ −93 mV, a value close to that measured in our electrophysiological recordings (see Fig. 4D) and normalized to the maximal conductance. Plotted points were fitted with a Boltzmann function: G/Gmax = 1 / [1 + exp(V$_{1/2}$ − V$_m$) / k] to yield the voltage for half-maximum activation (V$_{1/2}$) and the slope factor (k) values. To measure the channel kinetics, current traces were fitted with a single or a double exponential function of the following form: y = A$_{fast}$exp(τ / τ$_{fast}$) + A$_{slow}$exp(τ / τ$_{slow}$) (where A$_{fast}$ and A$_{slow}$ are the fractions of the fast and slow component of the current and τ$_{fast}$ and τ$_{slow}$ are the respective fast and slow time constant). The time constant representing the weighted average of the fast and slow components of current activation or deactivation was calculated with the following equation: τ = (τ$_{fast}$A$_{fast}$ + τ$_{slow}$A$_{slow}$) / (A$_{fast}$ + A$_{slow}$). Currents were analyzed using Origin 8.0 software. Analyses were performed after offline leak current subtraction. Membrane potentials were corrected for liquid junction potential (~5 mV).

Western blotting

One million CHO cells were transfected with 5 μg of pcDNA3-Kv7.2 (Kv7.2), pcDNA3-Kv7.2-p.A294V (Kv7.2^{A294V}), pcDNA3-Kv7.2-p.A294G (Kv7.2^{A294G}) or pcDNA3-Kv7.3 (Kv7.3) plasmids using the jetPEI® transfection reagent (Polyplus-transfection™) in 6 wells plate, according to the manufacturer's instructions. Forty-eight hours post-transfection, cells were washed three times with cold phosphate-buffered saline (PBS), then lysed with a lysis buffer containing 1% Triton-X100, 140 mM NaCl, 20 mM Tris, 2 mM EDTA pH 7.4, protease
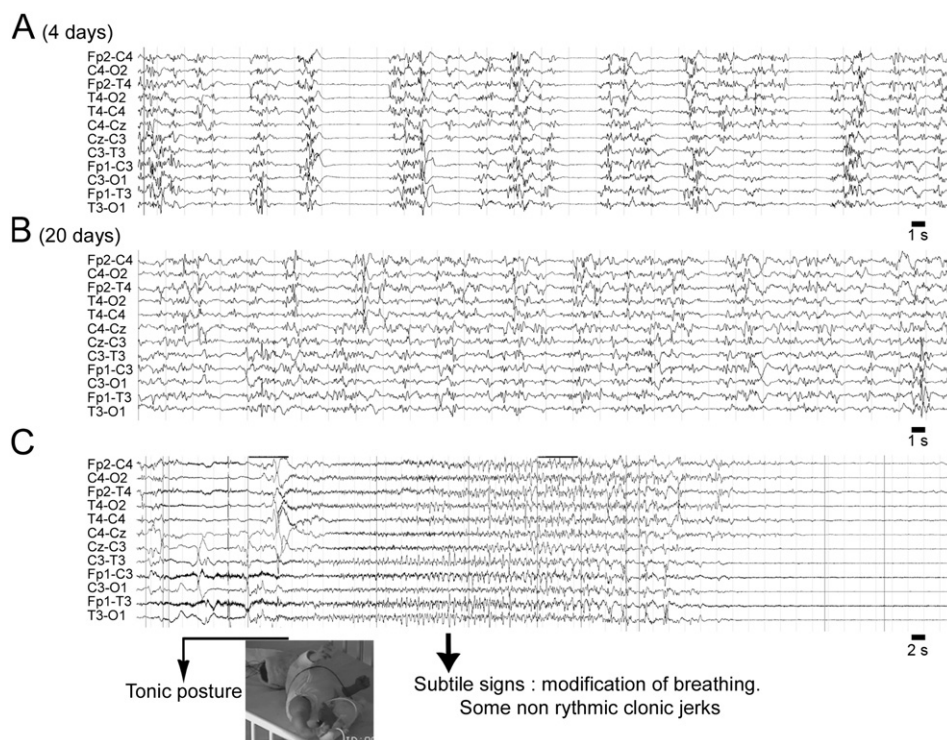

Fig. 2. Representative epileptic features during the neonatal period. A) First interictal EEG of patient 5 showing a suppression-burst pattern with bursts of activity that lasted longer than the silent periods, in average. The majority of the bursts was generalized to all the electrodes and was not associated with any movement. B) The interictal EEG tend to be more continuous, but still abnormal. C) Typical seizure recorded at day 5 (patient 5), with initial asymmetric tonic posture, while EEG shows generalized tonic discharge that seems to begin in the left hemisphere. Seizure was followed by a global flattening of the traces.

and phosphatase inhibitors (Pierce), for 30 min at 4 °C under agitation. Cells were then harvested and centrifuged at 13,000 g for 30 min. Denaturated samples were loaded on a SDS-PAGE tris–glycine gel. After migration, proteins were transferred onto a nitrocellulose membrane. Blots were saturated for 1 h in 5% non-fat milk in Tris-buffered saline (TBS) + Tween 0.05% and incubated overnight with a rabbit antisera against Kv7.2 (1:2000; Lonigro and Devaux, 2009), a rabbit antisera against Kv7.3 (1:2000), or anti-actin antibodies (1/2000; Sigma-Aldrich, ref. A5060). We washed the membranes three times with TBS + tween 0.05% and incubated the membranes for 1 h with 1:10,000 HRP conjugated secondary antibodies. Blots were revealed with Luminata forte (Millipore) and visualized with a Bio-Rad XRS system.

Hippocampal cell culture

Primary hippocampal cell cultures were prepared as previously described (Liu and Devaux, 2014). Neurons were transfected using Lipofectamine 2000 (Life Technologies) at 7 days in vitro (DIV) with V5-tagged Kv7.2 constructs together with hKv7.3 and pEGFP. For immunostaining, cells were fixed at DIV9 with 2% paraformaldehyde in PBS for 20 min at room temperature. Cells were washed three times in PBS, permeabilized with a solution containing 5% fish skin gelatin and 0.1% Triton X-100 in PBS for 30 min, then incubated for 1 h with rabbit antibodies against V5 (1:1000; V8137, Sigma-Aldrich) and mouse monoclonal antibodies against ankyrin-G (1:100; UC Davis/NINDS/NIMH NeuroMab Facility). The cells were then washed and revealed with the appropriate Alexa conjugated secondary antibodies (1:500; Jackson Immunoresearch) for 30 min. After several washes in PBS, cells were stained with DAPI, and mounted with Mowiol plus 4% DABCO (Sigma-Aldrich). Confocal image acquisition was performed on a Zeiss LSM780 laser scanning microscope equipped with a 63× (1.4 n.a.) oil immersion lens. Measurements were made on gray-scale confocal sections (8-bit) using ImageJ version 1.43u software (National Institutes of Health). Using the images of ankyrin-G staining, 20–30 μm long segments ("freehand" selection) were traced along the AIS then transferred to the images of V5 labeling for intensity measurements. Using GFP staining, regions of interest were manually selected in the middle of the soma (50 μm² square selection) or along proximal dendrites (20–30 μm long "freehand" selection) and were reported on the V5 staining for intensity measurements at soma and dendrites, respectively. Black pixels were eliminated (fluorescence = 0), and the mean pixel intensity per unit area was measured for each AIS, soma, and dendrite. Fluorescence ratios were calculated in 29 to 36 neurons for each construct. Digital images were processed into figures with Adobe Photoshop (Adobe Systems Inc.).
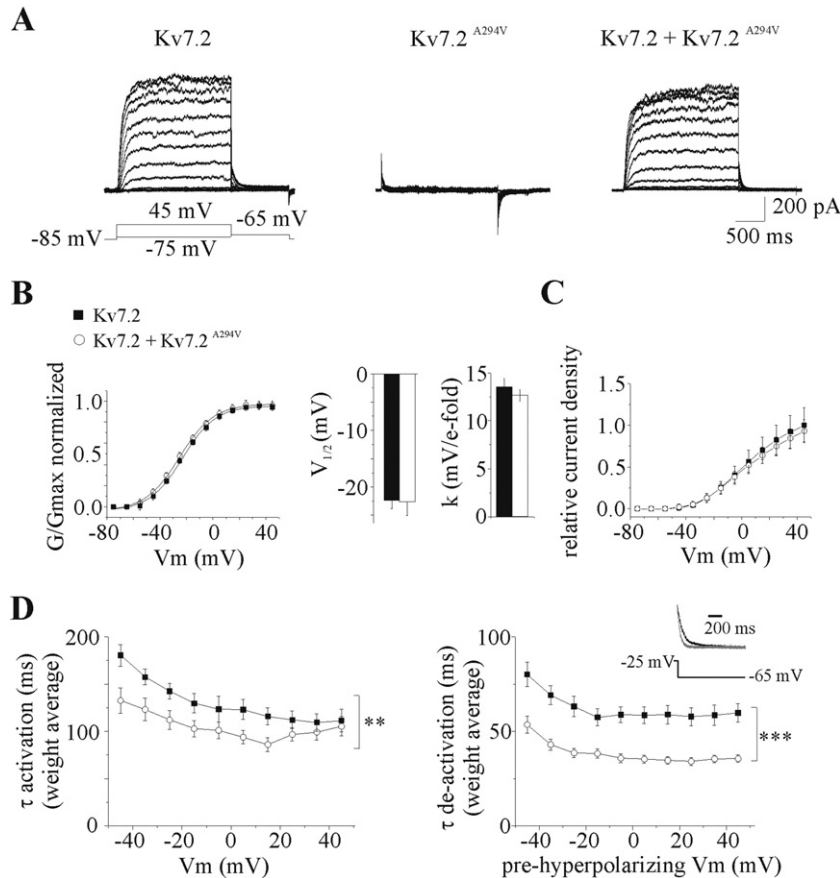

Fig. 3. Functional consequences of the pore p.A294V mutation on homomeric Kv7.2 channels. A) Current responses to 10 mV incremental depolarizing voltage step-command from −85 mV to +45 mV for 2 s followed by a 1 s hyperpolarizing voltage step to −65 mV in CHO cells transfected with wild-type Kv7.2 (left), Kv7.2^{A294V} (middle), and both Kv7.2^{A294V}/Kv7.2 (right). B) Conductance–voltage relationship of homomeric Kv7.2 channels (black square, n = 11 cells) and Kv7.2^{A294V}/Kv7.2 (empty circle, n = 11 cells) each normalized to their maximal conductance. Continuous lines represent Boltzmann fits to the experimental data. Histograms show the average of $V_{1/2}$ and slope factor (k) of homomeric Kv7.2 and Kv7.2^{A294V}/Kv7.2 channels calculated from 20 and 22 series of depolarizing voltage steps respectively. C) Relative current density measured at all voltage steps and showing that the mutation does not exert a dominant-negative effect. All values were normalized to the mean current density measured at 45 mV in CHO expressing the wild-type Kv7.2 subunit. D) Channel kinetics. Left: Weight average time constant of current activation measured at membrane potential (Vm) indicated in the abscissa. Homomeric Kv7.2 channels (wild-type or associated with the pore mutation) displayed a single exponential activation kinetic. Right: Weight average time constant of current deactivation of both channels. Vm indicated in the abscissa are values reached by the depolarizing voltage steps before the hyperpolarization to −65 mV. Superimposed traces in the inset are from (A) and represent tail currents after a step from −25 to −65 mV. They are scaled to show that the deactivation of the current in CHO expressing Kv7.2^{A294V}/Kv7.2 subunits (gray) is faster than that of wild-type Kv7.2 (black).

Statistical analysis

Data are represented as means ± s.e.m. When the data's distribution was normal, we used a Student's t-test to compare means of two groups or the one-way ANOVA followed by Bonferroni test as mentioned. When the normality test failed, we used the non-parametric Mann–Whitney test for two independent samples. Statistical analysis was performed using Graphpad Prism software. ns: not significant; *p < 0.05; **p < 0.01; and ***p < 0.001.

Results

The p.A294V mutation is associated with a severe clinical phenotype

Clinical and epileptic features of the patients are summarized in Tables 1 and 2. *KCNQ2* mutations were found *de novo*, except for two patients (1 and 6) who inherited the mutation from one mosaic parent. Clinical presentation at onset was notably stereotyped, with an initial stormy phase of epileptic seizures, mostly consisting of tonic asymmetric seizures beginning during the first days of life, and with a suppression-burst pattern on the interictal EEG (6/7 patients, Fig. 2). Epileptic activity stopped between 3 and 25 weeks of age in five patients, one patient died at 6 weeks (sudden unexpected death in epilepsy, SUDEP) and one patient was still epileptic at 12 years of age (Tables 1 and 2). Cessation of epilepsy was consecutive to sodium valproate administration in two patients, levetiracetam in one patient and phenytoin in one patient. Despite rapid offset of epilepsy in all patients but one, they all evolved to a severe phenotype. Only one patient was able to walk before 2 years of age but none of them acquired functional language. Overall, the phenotype associated with the recurrent Kv7.2^{A294V} mutation in our patient series was never benign and consisted mostly in an EOEE with a suppression-burst EEG pattern and poor developmental progression.

The p.A294V mutation has no dominant-negative effect on heteromeric Kv7.2/Kv7.3 channels

In a first set of experiments, CHO cells were transfected with plasmids expressing the wild-type Kv7.2 subunit to study homomeric Kv7.2 channels. Application of depolarizing voltage steps activated
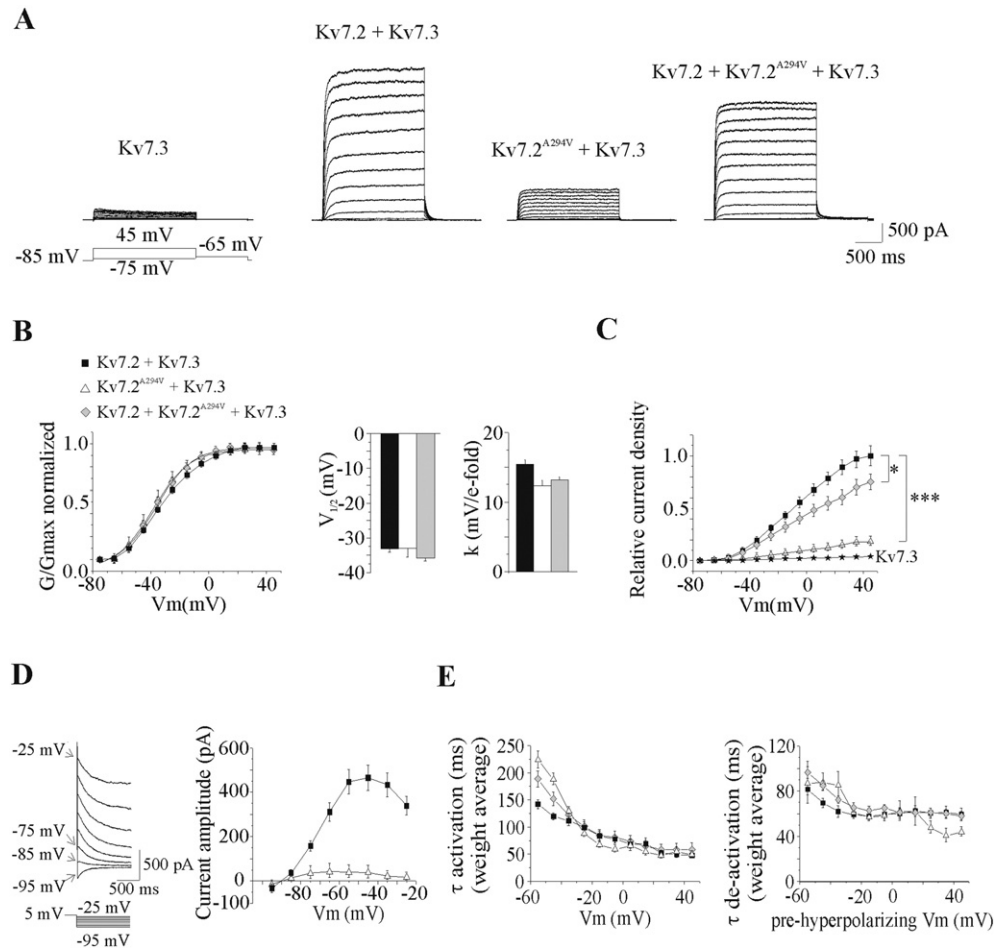

Fig. 4. Functional consequences of the pore p.A294V mutation on heteromeric channels. A) Representative current responses to depolarizing voltage steps observed in CHO cells transfected with Kv7.3 only; wild-type Kv7.2 + Kv7.3 (ratio 1:1); Kv7.2^{A294V} + Kv7.3 (ratio 1:1); Kv7.2^{A294V} + Kv7.2 + Kv7.3 (ratio 1:1:2) plasmids. B) Conductance–voltage relationships of wild-type heteromeric (black square, n = 25 cells), mutant heteromeric (open triangle, n = 14 cells) and mutant + wild-type heteromeric channels (gray diamond, n = 31 cells) normalized as in Fig. 2B. Averaged V$_{1/2}$ and k values are calculated from 42, 25 and 56 series of depolarizing voltage steps in the 3 conditions respectively. C) Relative current density measured in CHO cells transfected with the Kv7.3 (stars, n = 5) and with the different associations of Kv7.2 subunits. All values are normalized to the mean current density measured at +45 mV in CHO expressing the wild-type Kv7.2/Kv7.3 subunits. The slope of each graph was calculated after linear fit of data from −45 to +45 mV. The values are 0.0106, 0.0019 and 0.0075 for cells transfected with wild-type Kv7.2/Kv7.3, Kv7.2^{A294V}/Kv7.3 and Kv7.2^{A294V}/Kv7.2/Kv7.3 plasmids respectively. Thus, this pore mutation reduces by 83% and 30% M current density for the two last associations. D) Tail currents observed after a 1 s hyperpolarizing voltage step command from +5 mV to membrane potentials ranging from −25 mV to −95 mV. The amplitude of the currents were measured in cells expressing heteromeric wild-type subunits (black square) and Kv7.2^{A294V}/Kv7.3 subunits (open triangle) and plotted in the graph (left). Currents in both configurations reverse polarity at ~−90 mV, a value closed to the reversal potential calculated by Nernst equation. E) Channel kinetics. Weight average time constant of current activation (left) and deactivation (right). The mutation does not significantly impact the activation and deactivation processes (ANOVA followed by Bonferroni's test with multiple comparisons).

outward currents (Fig. 3A). Homomeric channels displayed a single exponential activation kinetic for currents evoked by depolarizing steps up to −10 mV and a double exponential for currents evoked by steps above −10 mV which accounted for 10–15% of the current activation process. Consistent with other studies (Maljevic et al., 2008; Orhan et al., 2014), the activation kinetic was voltage sensitive with time constant decreasing with the depolarization (Fig. 3D). Cell hyperpolarization to −65 mV leads to current deactivation which displayed a single exponential kinetic whatever the pre-hyperpolarizing membrane potential value (Fig. 3D). Full abolition of the current by XE-991 (10 μM, n = 3/3 cells, data not shown) confirmed the M current identity. Then, CHO cells were transfected either with Kv7.2^{A294V} expressing plasmid alone or with the Kv7.2^{A294V} and Kv7.2 subunits expressing plasmids in a 1:1 ratio. We did not observe any currents in cells transfected with the mutant subunit only (n = 8/8 cells, Fig. 3A). In contrast, in Kv7.2 + Kv7.2^{A294V} expressing cells, depolarizing voltage steps produced currents with a similar global density compared to those generated in homomeric Kv7.2 expressing CHO cells (Figs. 3A to C) but the kinetics of activation and deactivation were significantly faster for Kv7.2^{A294V}/Kv7.2 channels (p < 0.01 and p < 0.0001 respectively, Mann–Whitney test, Fig. 3D). These data indicated that Kv7.2^{A294V} does not exert a dominant-negative effect on wild-type Kv7.2. The Kv7.2^{A294V}/Kv7.2 association leads to the formation of a functional channel with significantly faster kinetics.

In a second series of experiments, we analyzed the functional impact of the Kv7.2^{A294V} subunit on heteromeric channels. Compared to homomeric Kv7.2 channels, the current density was ~4 times larger (176.5 ± 11.1 pA/pF, n = 45 cells and 43.4 ± 4.1 pA/pF, n = 30 cells measured at +45 mV for Kv7.2/Kv7.3 and Kv7.2 channels respectively) and the conductance–voltage relationship was shifted by ~10 mV to the left in cells expressing wild-type heteromeric Kv7.2/Kv7.3 channels (Figs. 3B, 4B, 5B, 6B). These effects are close to those already reported in CHO cells by Taglialatela's group (Soldovieri et al., 2006; Miceli et al., 2013). Moreover, heteromeric channels displayed a double

exponential deactivation kinetic with a slow time constant contributing to 20–25% of the current deactivation process. The co-transfection of Kv7.2^{A294V} with Kv7.3 in a 1:1 ratio generated currents reduced by ~83% compared to Kv7.2/Kv7.3 channels (ratio of the slope after linear fit of the data from −45 mV to +45 mV in the 2 configurations, n = 14 and 25 cells respectively, Figs. 4A to C). To ensure that co-transfection of Kv7.2^{A294V} and Kv7.3 leads to the formation of a functional heteromeric channel, we compared the current density measured at +45 mV in CHO cells transfected with Kv7.3 only versus Kv7.2^{A294V}/Kv7.3 subunits. We found a significant difference in the current density confirming the existence of a functional heteromeric channel (Kv7.3: 5.9 ± 1.1 pA/pF, n = 5 cells; Kv7.2^{A294V}/Kv7.3: 25.9 ± 2.3 pA/pF, n = 14 cells, p < 0.0001, Student's t-test, Figs. 4A, C). The conductance–voltage relationship, the activation and deactivation kinetics and the current reversal potential were not altered compared to Kv7.2/Kv7.3 channels (Figs. 4D, E). We then examined the impact of the Kv7.2^{A294V} subunit when co-expressed with Kv7.2 and Kv7.3 subunits in a 1:1:2 ratio (n = 31 cells), a ratio that is theoretically observed in patients. The current density produced in such a configuration was reduced by ~30% compared to Kv7.2/Kv7.3 channels, confirming that Kv7.2^{A294V} mutant does not exert a dominant-negative effect (Fig. 4C). As expected, there were no significant consequences on the conductance–voltage relationship and on channel kinetics (Figs. 4B, E).

Retigabine has similar enhancing action on wild-type and mutant channels

We then examined retigabine effect on heteromeric mutant channels. Retigabine has been marketed as an anti-epileptic drug for the treatment of resistant partial onset seizures and has been shown to enhance M current via its interaction with several specific residues located in S5 and S6 segments (Xiong et al., 2008; Lange et al., 2009; Orhan et al., 2014; Maljevic and Lerche, 2014). We wondered if the potentiating action of retigabine was affected by the p.A294V mutation. We used the same experimental procedure as above but depolarizing
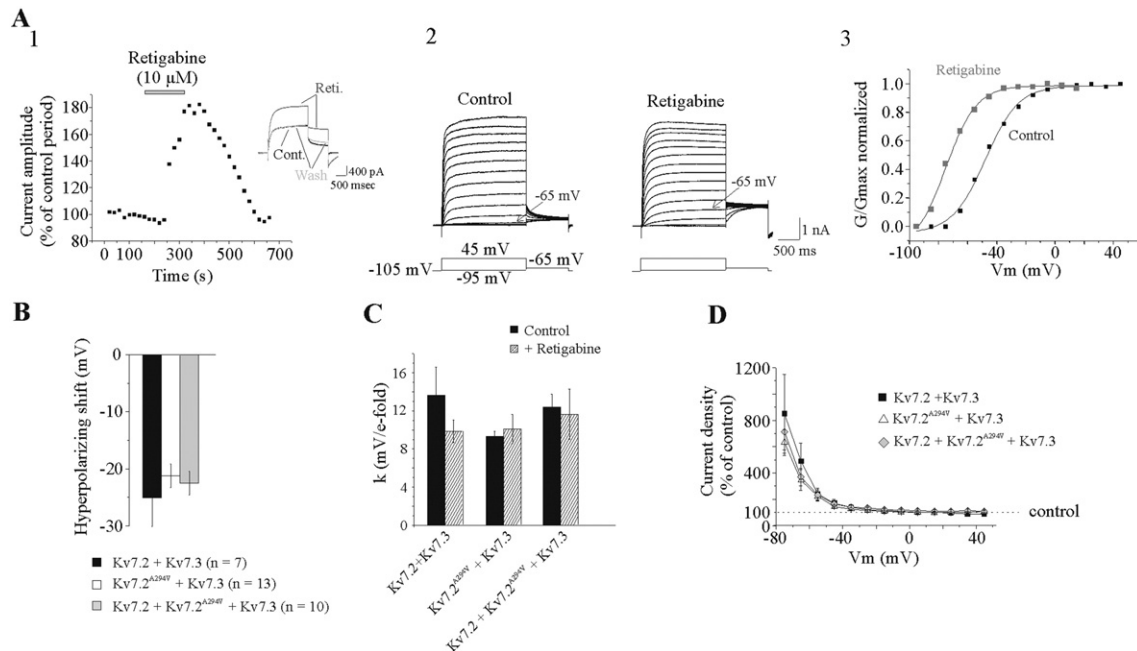

Fig. 5. The enhancing effect of retigabine on M current is not affected by the p.A294V mutation. A1) Representative experiment showing the time course of the effect of retigabine (10 μM) on heteromeric wild-type channels Kv7.2/Kv7.3. The current is evoked every 20 s by a constant depolarizing voltage step command from −105 mV to −45 mV. Inset depicted currents evoked just before bath application of retigabine, at the end of drug application, and after retigabine washout. Leak current have not been subtracted. A2) Current responses to incremental depolarizing voltage steps command from −105 mV to −45 mV performed in the same cell before the application of retigabine (control) and before the washout of the drug (retigabine). A3) Corresponding conductance–voltage relationships, each normalized to their maximal conductance. B–C) Summary of the effect of retigabine on the hyperpolarizing shift of channels G–V relationships (B, ANOVA followed by Bonferroni's test with multiple comparisons) and slope factor (C, Student's t-test, control vs retigabine) resulting from the association of subunits indicated below the histograms. D) Summary of retigabine effect on current density expressed as percentage of control (period preceding the application of the drug for each cells). The mutation does not impair the voltage sensitive enhancing action of retigabine.

voltage steps were applied from a holding membrane potential of −105 mV. Fig. 5A shows the typical effect of retigabine in a cell expressing heteromeric wild-type channels. Bath application of retigabine (10 μM) rapidly and reversibly enhanced M current amplitude in a voltage sensitive manner as shown previously (Xiong et al., 2008). Retigabine also produced a 25 mV ± 5 mV hyperpolarizing shift of $V_{1/2}$ with no significant change in the slope factor (Figs. 5B to D). Similar effects of retigabine were observed in CHO cells expressing heteromeric mutant channels, including the hyperpolarizing shift of $V_{1/2}$ and the voltage dependent increase in current density. Thus, the potentiating effect of retigabine was maintained on mutated heteromeric channel and indicated that Ala-294 residue in the segment S6 is not crucial for the binding of retigabine.

The p.A294G mutation reduces global current density of the heteromeric channels to the same extent as the p.A294V mutation

In order to determine whether these alterations were specific to EOEE mutations, we then performed the same types of experiments for the Kv7.2^{A294G}, a mutation associated with BFNS and affecting the same residue. As shown in Fig. 6, this mutation did not have any significant consequences on M current characteristics ($V_{1/2}$, k factor, current density and kinetics) in CHO cells expressing the homomeric mutant channels (n = 17 cells) or expressing the Kv7.2^{A294G}/Kv7.2 subunits (n = 16 cells) compared to wild-type homomeric channels (n = 19 cells). In contrast, the p.A294G mutation affected the current in cells co-expressing the mutant subunit and Kv7.3 (Fig. 7). The global current

density of Kv7.2^{A294G}/Kv7.3 expressing cells was reduced by ~50% compared to those expressing heteromeric wild-type channels (n = 19 and 20 cells respectively, Fig. 7C). This was not accompanied by a change in the conductance–voltage relationship although there was a small reduction of the slope factor (Fig. 7B). The deactivation kinetic of the mutant channel was also slightly but significantly slower than that of the heteromeric wild-type channels whereas the activation kinetic was globally unchanged (Fig. 7D). The co-expression of the wild-type Kv7.2 subunit with Kv7.2^{A294G} and Kv7.3 (n = 20 cells) led to channels with similar activation properties and deactivation kinetics than heteromeric wild-type channels. However, the global current density was only partially restored and still remained ~30% less than that of Kv7.2/Kv7.3 expressing cells. Therefore the p.A294G mutation reduces the global current density to the same extent than the p.A294V mutation in the configuration that mimics the situation in patients.

Mutation of Ala294 affects the expression level of homomeric but not heteromeric mutant channels in CHO cells

We next analyzed the impact of the Ala294 residue mutation on protein expression in CHO cells by western blot analysis. First, we measured the total amount of Kv7.2 proteins and compared the amount of wild-type versus p.A294V mutated subunits (Figs. 8A, B). We found that total Kv7.2^{A294V} expression level was reduced by ~80% compared to that of Kv7.2; this decrease was fully rescued by co-expression with Kv7.3. We then performed the same experiments after co-transfection of Kv7.2^{A294G} in CHO cells. As for Kv7.2^{A294V}, the p.A294G mutation
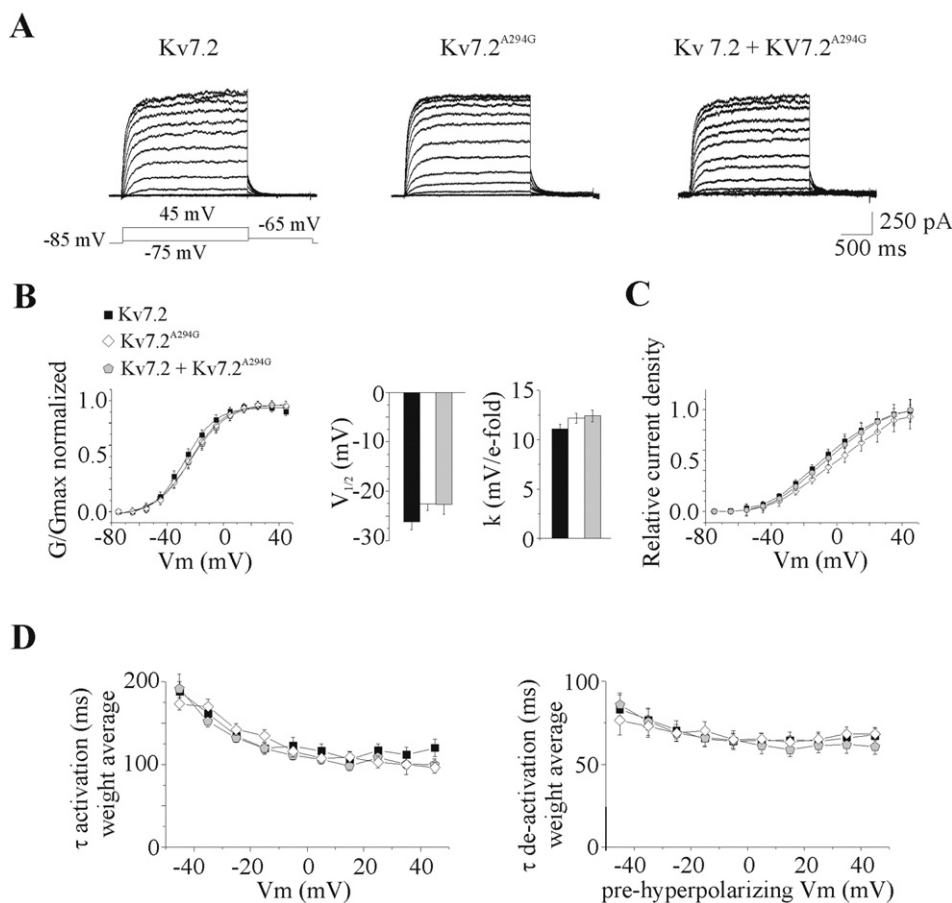

Fig. 6. Functional consequences of the pore p.A294G mutation on homomeric Kv7.2 channels. A) Representative current responses to depolarizing voltage steps observed in CHO cells transfected with wild-type Kv7.2 (left), Kv7.2^{A294G} (middle); Kv7.2 + Kv7.2^{A294G} (ratio 1:1 right) plasmids. B) Conductance–voltage relationships of wild-type homomeric (black square, n = 19 cells), mutant heteromeric (open diamond, n = 17 cells) and mutant + wild-type heteromeric channels (gray pentagon, n = 16 cells) normalized as in Fig. 3B. Averaged $V_{1/2}$ and k values are calculated from 35, 34 and 31 series of depolarizing voltage steps in the three conditions respectively. C) Relative current density measured in CHO cells transfected in the three different conditions. Values are normalized as in Fig. 3C. D) Weight average time constant of current activation (left) and deactivation (right).

affected channel expression, albeit to a much lower level than p.A294V (40% of wild-type expression). Again, the Kv7.3 subunit was able to restore the total Kv7.2^{A294G} expression to wild-type levels (Figs. 8C, D). This suggests that the assembly of both mutant subunits with Kv7.3 prevents the degradation of the mutated protein and that conservation of the Ala294 residue is important for the stability of the Kv7.2 subunit.

The p.A294V but not the p.A294G mutation induced a redistribution of Kv7 channels to the somato-dendritic compartment

After the consequence analyses of the p.A294V and p.A294G mutations on Kv7 channel properties and expression in CHO cells, we went on to test whether this mutation could affect the distribution of Kv7 channels in hippocampal neurons. For this purpose, cultured hippocampal neurons were transfected at DIV7 with V5-tagged Kv7.2 constructs in combination with Kv7.3 and GFP to assess neuronal morphology. Neurons were then immunostained 48 h later for V5 and for ankyrin-G to label the AIS (Fig. 9A). As previously described, wild-type Kv7.2/Kv7.3 heteromers were concentrated at the AIS and co-localized with ankyrin-G (Devaux et al., 2004; Chung et al., 2006; Pan et al.,

2006; Rasmussen et al., 2007; Liu and Devaux, 2014; Cavaretta et al., 2014). By contrast, the co-expression of the Kv7.2^{A294V} with Kv7.3 or with wild-type Kv7.2/Kv7.3 strongly affected the distribution of the heteromeric channels in neurons and resulted in the loss of the axonal regionalization of Kv7 subunits (Figs. 9B to C). In order to quantify these alterations, we measured the mean fluorescence intensity of V5 staining at the AIS and compared it with the dendrites and soma (Fig. 9F). This demonstrated that the density not only of mutant Kv7.2 channels, but also that of wild-type and mutant Kv7.2 channels, was significantly decreased at the AIS. The mutant heteromers were instead mostly detected in the somato-dendritic compartment leading to a strong and significant decrease in the AIS/dendrite and AIS/soma ratios of fluorescence for Kv7.2^{A294V}/Kv7.3 (~60% decrease; V5-tagged Kv7.2^{A294V}) and Kv7.2^{A294V}/Kv7.2/Kv7.3 (~48% decrease; V5-tagged Kv7.2) compared to Kv7.2/Kv7.3 (V5-tagged Kv7.2) (Fig. 9F). Interestingly, these diminutions were not significantly different from each other. In contrast, the distribution of Kv7 channels carrying the p.A294G mutation was similar to that of wild-type channels with a strong concentration of the Kv7.2^{A294G}/Kv7.3 or Kv7.2^{A294G}/Kv7.2/Kv7.3 at the AIS (Figs. 9D–E) and no alterations of the AIS/dendrite or AIS/soma ratios (Fig. 9F).
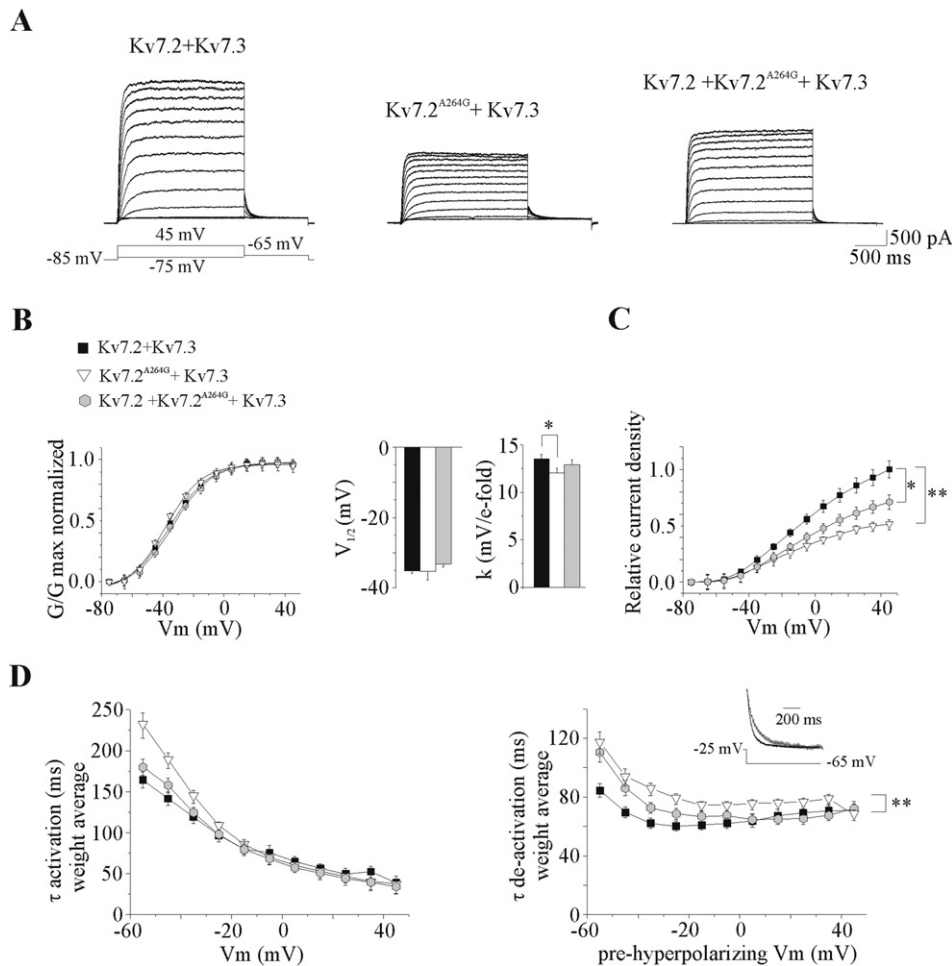

Fig. 7. Functional consequences of the pore p.A294G mutation on heteromeric channels. A) Representative current responses to depolarizing voltage steps observed in CHO cells transfected with wild-type Kv7.2 + Kv7.3 (ratio 1:1, left); Kv7.2^{A294G} + Kv7.3 (ratio 1:1, middle); Kv7.2 + Kv7.2^{A294G} + Kv7.3 (ratio 1:1:2, right) plasmids. B) Conductance–voltage relationships of wild-type heteromeric (black square, n = 19 cells), mutant heteromeric (white triangle, n = 20 cells) and mutant + wild-type heteromeric channels (gray hexagon, n = 20 cells). Averaged V$_{1/2}$ and k values are calculated from 38, 37 and 40 series of depolarizing voltage steps in the three conditions respectively. C) Relative current density measured in CHO cells transfected with the three different associations of plasmids. Values are normalized as in Fig. 3C. The slope of each graph was calculated after linear fit of data from −45 to +45 mV. The values are 0.0103, 0.0051 and 0.0074 for cells transfected with wild-type Kv7.2/Kv7.3, Kv7.2^{A294G}/Kv7.3 and Kv7.2^{A294G}/Kv7.2/Kv7.3 plasmids respectively. This pore mutation reduces by 50% and 29% M current density for the two last associations. D) Weight average time constant of current activation (left) and deactivation (right). Superimposed traces in the inset are from (A) and represent tail currents after a step from −25 to −65 mV. They are scaled to show that the deactivation of the currents in CHO expressing Kv7.2^{A294G}/Kv7.3 subunits (gray) are slower than that of wild-type Kv7.2/Kv7.3 (black).
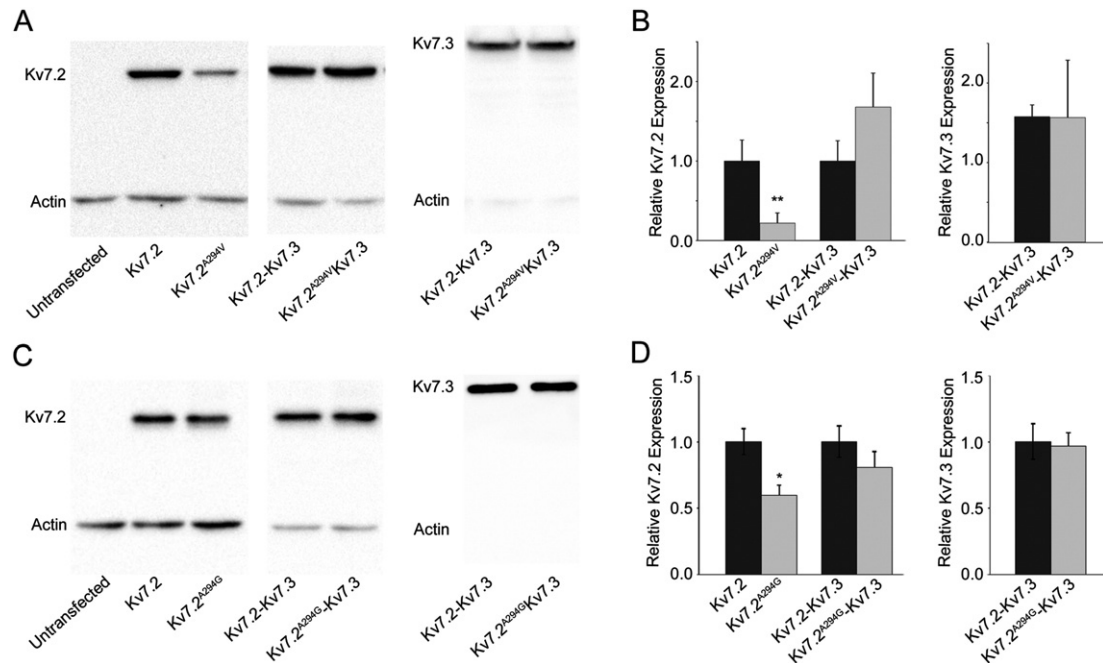
Fig. 8. The two pore p.A294V and p.A294G mutations affect the expression of homomeric but not of heteromeric mutant channels in CHO cells. We performed western blot analysis by revealing Kv7.2 (92 kDa), Kv7.3 (96 kDa) or actin (42 kDa), as loading control (A, left and middle) western blot analysis of total input of untransfected, transfected CHO cells with Kv7.2 or Kv7.2^{A294V}, with Kv7.2/Kv7.3 or Kv7.2^{A294V}/Kv7.3 revealed with a Kv7.2 antibody. (A, right) Same blot as middle treated with stripping buffer and reprobed with the Kv7.3 antibody only. Note that Kv7.3 prevents Kv7.2^{A294V} degradation. (B) Total protein expression was analyzed by normalizing total Kv7.2 to the corresponding actin signal. We performed 6 and 7 independent experiments for homo and heteromeric channels respectively (Mann–Whitney test). (C–D) Comparison of Kv7.2^{A294G} subunit expression as in A and B. For this mutation, we performed 5 and 4 independent experiments for homomeric and heteromeric channels respectively (Mann–Whitney test).
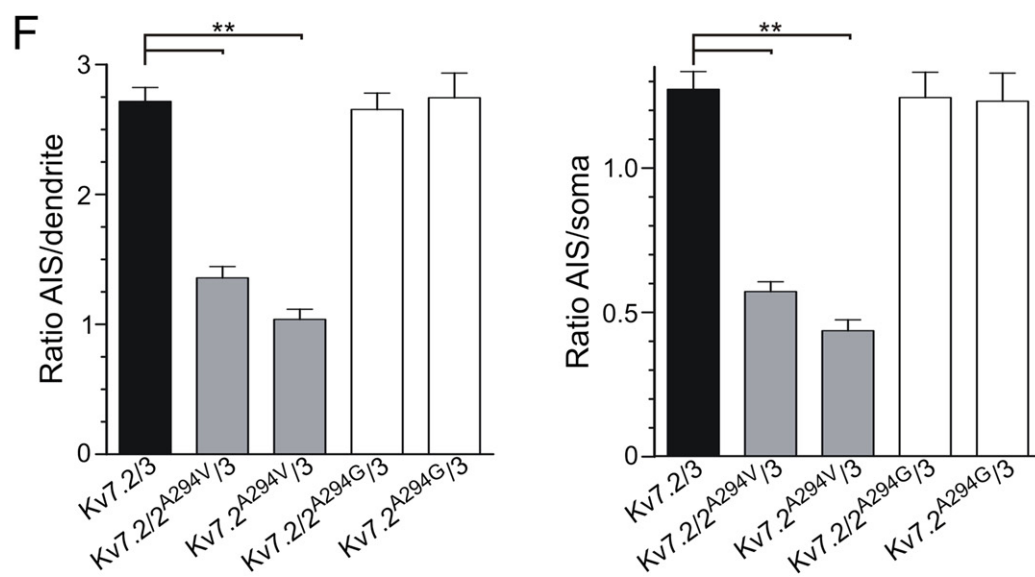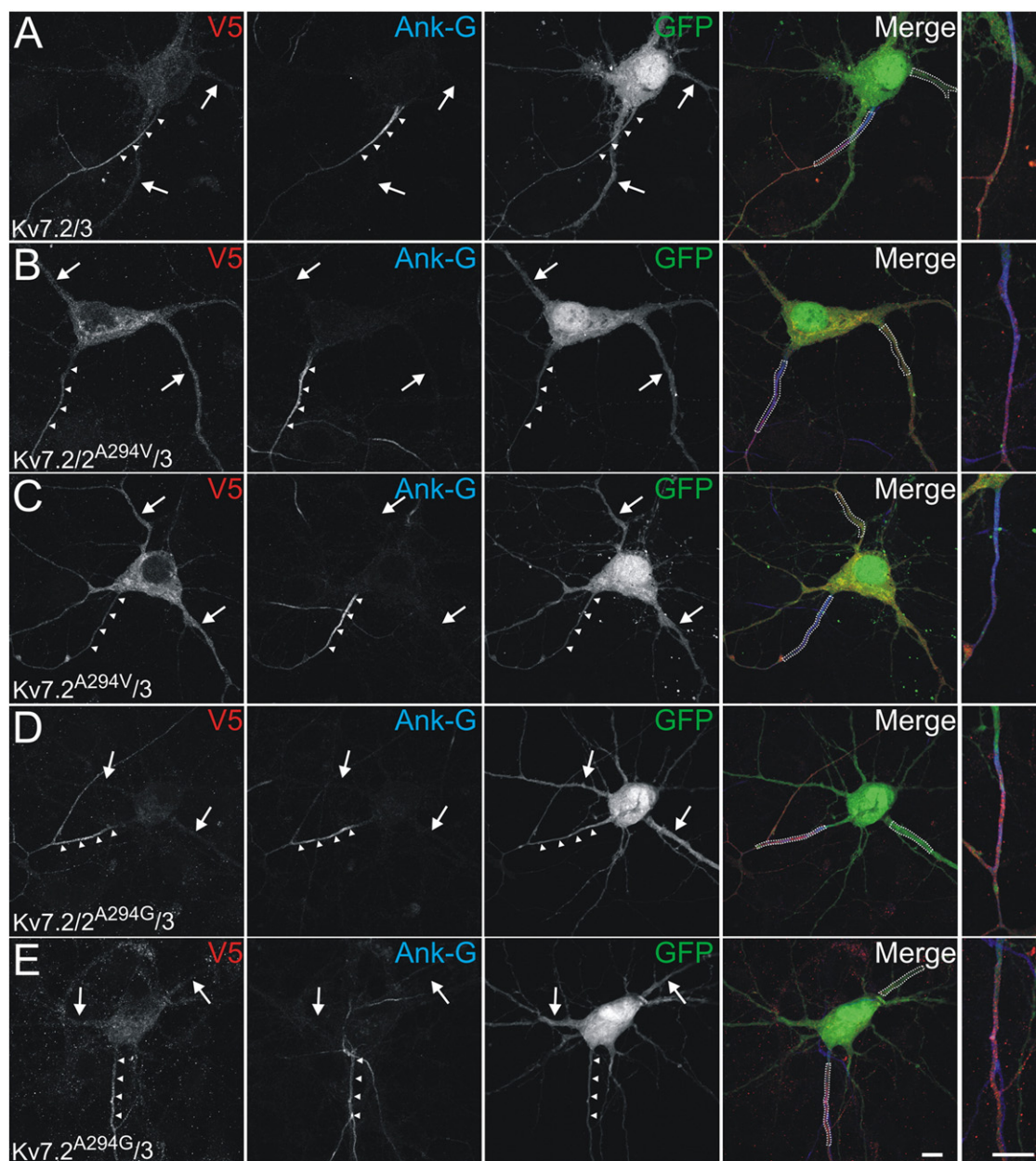
Discussion

Mutations in *KCNQ2* lead to neonatal epilepsies that have drastically different prognoses, ranging from benign (BFNS) to severe (EOEE) evolutions in children with *KCNQ2*-related epilepsy. With rare exceptions (Borgatti et al., 2004; Steinlein et al., 2007), most of the *KCNQ2* mutations associated with BFNS are, to date, distinct from those found in EOEE. Therefore, the variability of *KCNQ2*-related epileptic phenotypes could be a direct consequence of the functional alterations in the M-current, which then would be predictive of the patients' neurological evolution. Here, we studied the recurrent p.A294V mutation located in the S6 segment of the protein that we identified in 7 patients; we compared its functional consequences with those of the p.A294G mutation, an inherited mutation associated with BFNS (Steinlein et al., 2007). First, the electro-clinical features and clinical evolution of the patients carrying the mutation p.A294V were characteristic of an EOEE. Although we found some degree of variability in the neurological evolution, all patients described here had a severe encephalopathy with intellectual disabilities and/or motor impairments. A similar phenotype was associated with the same mutation in three previously reported patients (Kato et al., 2013; Allen et al., 2014). Thus, p.A294V is a frequent mutation that gives rise to a severe form of neonatal epilepsy, mostly associated with an initial suppression-burst pattern of the EEG, profound motor and cognitive impairment despite the short course of epilepsy.

Second, we observed that the mutation of the Ala294 residue has functional consequences on Kv7 channels. No currents were detected in cells expressing the Kv7.2^{A294V} subunit only and the current amplitude was reduced when this mutant or the Kv7.2^{A294G} subunit was co-expressed with wild-type Kv7.3 or Kv7.2/Kv7.3 subunits. Given the important role played by M current not only in controlling cortical network activities in adult but also in the developing brain (Peters et al., 2005; Safiulina et al., 2008), it is likely that the reduction of current density may be one important cause in both diseases. However, M current density was similarly reduced by 30%, when each mutant was co-expressed with Kv7.2/Kv7.3 subunits in a 1:1:2 ratio, supposed

to replicate the expression ratio existing in patients. This reduction amplitude is close to that reported for most of *KCNQ2*-related BFNS mutations (~25–30%, Maljevic et al., 2008; Maljevic and Lerche, 2014; Soldovieri et al., 2014) and that observed with the p.A294G mutation. Therefore, while the clinical consequences of the p.A294V mutation are severe, its impact on the M current is moderate, suggesting that this mutation may act through other mechanisms than a simple functional alteration. Our study contrasts with other studies in which mutations associated with EOEE and located in the pore region or S4 segment have dominant-negative effects and reduce current density by 50–70% (Miceli et al., 2013; Orhan et al., 2014). However, Orhan and collaborators also reported two other EOEE mutations localized in the C-terminal domain of Kv7.2 subunit (p.M518V and p.R532W) characterized by global M current densities reduced by only 25%. Therefore, in accordance with the present study, we postulate that the degree of M current inhibition, measured in non-neuronal expressing systems, is not always predictive of the disease severity. This is further supported by a very recent study showing even a gain of function induced by mutations located in the voltage sensor domain and associated with EOEE (Miceli et al., 2015).

We also observed that the p.A294V mutation reduced the total expression of Kv7.2 subunits by ~80%, while the protein was normally expressed in cells co-transfected with the mutant and Kv7.3 subunits. This suggests that the mutation could alter protein folding and/or increase endoplasmic reticulum degradation and that the association of the mutant subunit with Kv7.3 may be protective. Such a protective effect of Kv7.3 has also been described on the c.2043ΔT frameshift mutation located in the C-terminal domain of Kv7.2 (Coppola et al., 2003; Soldovieri et al., 2006). In our study, in spite of the restoration of Kv7.2^{A294V} protein to wild-type levels, current density in cells co-expressing Kv7.2^{A294V}/Kv7.3 was strongly reduced (~80%) compared to wild-type heteromeric channel. In contrast to the p.A294V mutation, we did not observe any effect of the p.A294G mutation on the homomeric Kv7.2 channel, although we found an ~40% decrease in total channel expression by western blotting. The pA294G channel

A V5 | Ank-G | GFP | Merge
Kv7.2/3

B V5 | Ank-G | GFP | Merge
Kv7.2/2^{A294V}/3

C V5 | Ank-G | GFP | Merge
Kv7.2^{A294V}/3

D V5 | Ank-G | GFP | Merge
Kv7.2/2^{A294G}/3

E V5 | Ank-G | GFP | Merge
Kv7.2^{A294G}/3

F

Ratio AIS/dendrite **

Kv7.2/3 | Kv7.2/2^{A294V}/3 | Kv7.2^{A294V}/3 | Kv7.2/2^{A294G}/3 | Kv7.2^{A294G}/3

Ratio AIS/soma **

Kv7.2/3 | Kv7.2/2^{A294V}/3 | Kv7.2^{A294V}/3 | Kv7.2/2^{A294G}/3 | Kv7.2^{A294G}/3

appears less sensitive to intracellular degradation than the pA294V channel, and more efficient at reaching the cell membrane by itself since it generates a current identical to that of the wild-type Kv7.2 subunit. However, in the situation where Kv7.2 is expressed with Kv7.3 and a mutated subunit, both mutations behave similarly and lead to an equivalent decrease in M current, thus unmasking the functional impairment in Kv7.2^{A294G}. This suggests that Ala294 may be an important residue for pore formation and heteromeric channel activity. As a consequence, the bulkier Val residue in Kv7.2^{A294V} would be more deleterious than the smaller Gly in Kv7.2^{A294G}.

The heterologous expression in hippocampal neurons further indicated that the p.A294V but not the p.A294G mutation strongly affects the neuronal localization of Kv7.2^{A294V}/Kv7.3 channels. In neurons, channel composed of p.A294V mutated subunit presented a decreased density at the AIS and were mostly detected within the somato-dendritic compartment. Interestingly, the decrease in AIS/dendrite ratio was not significantly different in neurons transfected with Kv7.2^{A294V}/Kv7.3 or with Kv7.2^{A294V}/Kv7.2/Kv7.3, indicating that wild-type Kv7.2 or Kv7.3 subunits were not able to restore the normal location of the channels. Axonal targeting defects have also been described in some BFNS cases (Chung et al., 2006; Cavaretta et al., 2014; Liu and Devaux, 2014). However, to our knowledge, such influence exerted by a mutant subunit on the heteromeric channel targeting has never been described in severe KCNQ2-related epilepsies and in configuration mimicking the patients' heterozygous genotype. It is although unclear how the p.A294V mutation may selectively affect the axonal targeting of M channels. Indeed, molecules involved in channels targeting, such as calmodulin and ankyrin-G, bind the C-terminus of Kv7.2 subunit (Devaux et al., 2004; Pan et al., 2006; Rasmussen et al., 2007; Etxeberria et al., 2008; Liu and Devaux, 2014; Cavaretta et al., 2014), including the proximal domain (amino acids 323–500) but not the segment S6. Therefore, our current hypothesis is that the substitution of Ala294 by valine, but not by glycine residue, indirectly affects the binding of regulatory proteins involved in channel targeting to the C-terminal domain or even at position 294 of Kv7.2.

This new data provides an additional mechanism that could play a crucial role in the severity of the disease, although the electrophysiological consequences may be complex. Indeed, while a decreased expression and a reduced current density at the AIS may favor neuronal firing (Yue and Yaari, 2006; Hu et al., 2007; Shah et al., 2008; Battefeld et al., 2014; Soh et al., 2014), an increase in channel expression at the dendritic level may lower the dendritic input resistance, dampening dendrite excitability. Further studies are required to understand the functional consequences of this dendritic localization of Kv7 channels with a specific attention on synaptic integration of excitatory inputs and temporal summation of excitatory post-synaptic potentials that are likely to be impacted by this channel redistribution (Magee, 2000; Shah et al., 2011). In contrast, for the BFNS mutation A294G, our data suggest that this mutation might affect the function of the heteromeric channels in their normal neuronal location (i.e., the AIS).

How could we treat the patients? Recently, the interest in retigabine as a potential treatment was raised for some KCNQ2 mutations altering the current density. However, it is likely that retigabine is of lesser interest here, since the main effect of KCNQ2 mutation we observed was on channel targeting and not on I_M current (with Kv7.2^{A294V}/Kv7.2/Kv7.3), and that such a treatment may potentially induce a more important dampening of dendritic excitability. Carbamazepine has been shown to be effec-tive in some KCNQ2-related epileptic encephalopathies (Kato et al., 2013; Numis et al., 2014). Here, we cannot clearly attribute the cessation of epilepsy to any particular anti-epileptic drug since very different protocols were used for each patient. However, we confirmed that the neurological prognosis may be very poor despite the short duration of the epilepsy (Kato et al., 2013; Milh et al., 2013). This would tend to confirm that neurological disability is not just a sequel of neonatal seizures and raise the question of the appropriateness of the term "epileptic encephalopathy" to characterize the severe forms of KCNQ2-related epilepsies. More than the epileptic and/or interictal activity per se, the KCNQ2 "channelopathy" may cause a developmental impairment via permanent disruption of neuronal networks. In theory, the effects of the p.A294V mutation could be reduced using molecules preventing the targeting of the channel to the somato-dendritic compartment. To our knowledge, such molecules have not yet been uncovered. A better understanding of Kv7.2 targeting and pre-clinical pharmacological studies remains instrumental to develop new treatments.

Conclusions

We conclude that p.A294V is a frequent mutation that always gives rise to a severe phenotype. This mutation has a strong impact on the mutant subunit expression and its function. In a configuration that is theoretically observed in patients, the mutant subunit reduces global current density to the same extent as a BFNS mutation involving the same residue. However, we found that the p.A294V mutation specifically affects the targeting of the channel to the AIS. To our knowledge, such an effect has never been described for previously documented KCNQ2 mutations. Altogether, we suggest that the disease severity may not necessarily result from a strong impairment of the M current and it is likely that the reorganization of channel distribution is also important. Therefore, the subcellular analysis of Kv7 channel expression should be taken into consideration for future studies on KCNQ2 mutations and future treatment development.

Appendix A. Supplementary data

Supplementary data to this article can be found online at http://dx.doi.org/10.1016/j.nbd.2015.04.017.

Fig. 9. The pore p.A294V mutation increases Kv7 channels expression in the somato-dendritic compartment.(A–E) Hippocampal neurons (DIV9) were transfected with GFP (green) and V5-tagged Kv7.2 (A), Kv7.2^{A294V}/Kv7.2 (B), Kv7.2^{A294V} (C), Kv7.2^{A294G}/Kv7.2 (D) or Kv7.2^{A294G} (E) together with Kv7.3 constructs, then were immunostained for V5 (red) and ankyrin-G (blue) to label the AIS (arrowheads). Wild-type Kv7.2/Kv7.3 channels are selectively addressed at the AIS and co-localize with ankyrin-G. The heteromeric association of the mutant Kv7.2^{A294V} subunit with wild-type Kv7.3 or Kv7.2/Kv7.3 subunits leads to a reduction in the fluorescence density at the AIS. Instead, the mutant channels are predominantly localized in the somato-dendritic compartment (arrows). By contrast, the heteromeric association of the mutant Kv7.2^{A294G} subunit with wild-type Kv7.3 or Kv7.2/Kv7.3 subunits did not affect the localization of the channels at AIS. Isolated AIS labeling are shown at a higher magnification in the left panels. F) The intensity of V5 staining was measured along a 20–30 μm long selection (dashed lines) within the AIS, dendrites and soma, and the fluorescence ratio AIS/dendrite and AIS/soma were calculated (n = 29 to 36 neurons from 4 different sets of experiments for each condition). ANOVA followed by Bonferroni's test with multiple-comparisons. Scale bars: 10 μm.

References

Allen, N.M., Mannion, M., Conroy, J., Lynch, S.A., Shahwan, A., Lynch, B., King, M.D., 2014. The variable phenotypes of KCNQ-related epilepsy. Epilepsia 55, 99–105.

Battefeld, A., Tran, B.T., Gavrilis, J., Cooper, E.C., Kole, M.H., 2014. Heteromeric Kv7.2/7.3 channels differentially regulate action potential initiation and conduction in neocortical myelinated axons. J. Neurosci. 34, 3719–3732.

Biervert, C., Schroeder, B.C., Kubisch, C., Berkovic, S.F., Prooing, P., Jentsch, T.J., Steinlein, O.K., 1998. A potassium channel mutation in neonatal human epilepsy. Science 279, 403–406.

Borgatti, R., Zucca, C., Cavallini, A., Ferrario, M., Panzeri, C., Castaldo, P., Soldovieri, M.V., Baschirotto, C., Bresolin, N., Dalla Bernardina, B., Tagalialatela, M., Bassi, M.T., 2004. A novel mutation in KCNQ2 associated with BFNC, drug reistant epilepsy, and menral retardation. Neurology 63, 57–65.

Brown, D.A., Passmore, G.M., 2009. Neural KCNQ (Kv7) channels. Br. J. Pharmacol. 156, 1185–1195.

Cavaretta, J.P., Sherer, K.R., Lee, K.Y., Kim, E.H., Issema, R.S., Chung, H.J., 2014. Polarized axonal surface expression of neuronal KCNQ potassium channels is regulated by calmodulin interaction with KCNQ2 subunit. PLoS One 9, e103655.

Charlier, C., Singh, N.A., Ryan, S.G., Lewis, T.B., Reus, B.E., Leach, R.J., Leppert, R.M., 1998. A pore mutation in a novel KQT-like potassium channel gene in an idiopathic epilepsy family. Nat. Genet. 18, 53–55.

Chung, H.J., Jan, Y.N., Jan, L.Y., 2006. Polarized axonal surface expression of neuronal KCNQ channels is mediated by multiple signals in the KCNQ2 and KCNQ3 C-terminal domains. Proc. Natl. Acad. Sci. U. S. A. 103, 8870–8875.

Coppola, G., Castaldo, P., Miraglia del Giudice, E., Bellini, G., Galasso, F., Soldovieri, M.V., Anzalone, L., Sferro, C., Annunziato, L., Pascotto, A., Tagalialatela, M., 2003. A novel KCNQ2 K+ channel mutation in benign neonatal convulsions and centrotemporal spikes. Neurology 61, 131–134.

Dalen Meurs-van der Schoor, C., van Weissenbruch, M., van Kempen, M., Bugiani, M., Aronica, E., Ronner, H., Vermeulen, R.J., 2014. Severe neonatal epileptic encephalopathy and KCNQ2 mutation: neuropathological substrate? Front. Pediatr. 2, 136.

Devaux, J.J., Kleopa, K.A., Cooper, E.C., Scherer, S.S., 2004. KCNQ2 is a nodal K+ channel. J. Neurosci. 24, 1236–1244.

Etxeberria, A., Aivar, P., Rodriguez-Alfaro, J.A., Alaimo, A., Villace, P., Gomez-Posada, J.C., Areso, P., Villaroel, A., 2008. Calmodulin regulates the trafficking of KCNQ2 potassium channels. FASEB J. 22, 1135–1143.

Hu, H., Vervaeke, K., Storm, J.F., 2007. M-channels (Kv7/KCNQ channels) that regulate synaptic integration, excitability, and spike pattern of CA1 pyramidal cells are located in the perisomatic region. J. Neurosci. 27, 1853–1867.

Jentsch, T.J., 2000. Neuronal KCNQ potassium channels: physiology and role in disease. Nat. Rev. Neurosci. 1, 21–30.

Kato, M., Yamagata, T., Kubota, M., Arai, H., Yamashita, S., Nakagawa, T., Fujii, T., Imai, K., Uster, T., Chitayat, D., Weiss, S., Kashii, H., Kusano, R., Matsumoto, A., Nakamura, K., Oyazato, Y., Maeno, M., Nishiyama, K., Kodera, H., Nakashima, M., Tsurusaki, Y., Miyake, N., Saito, K., Hayasaka, K., Matsumoto, N., Saitsu, H., 2013. Clinical spectrum of early onset epileptic encephalopathies caused by KCNQ2 mutation. Epilepsia 54, 1282–1287.

Lange, W., Geissendörfer, J., Schenzer, A., Grötzinger, J., Seebohm, G., Friedrich, T., Schwake, M., 2009. Refinement of the binding site and mode of action of the anticonvulsant Retigabine on KCNQ K+ channels. Mol. Pharmacol. 275, 272–280.

Liu, W., Devaux, J.J., 2014. Calmodulin orchestrates the heteromeric assembly and the trafficking of KCNQ2/3 (Kv7.2/3) channels in neurons. Mol. Cell. Neurosci. 58, 40–52.

Lonigro, A., Devaux, J.J., 2009. Disruption of neurofascin and gliomedin at nodes of Ranvier precedes demyelination in experimental allergic neuritis. Brain 132, 260–273.

Magee, J.C., 2000. Dendritic integration of excitatory synaptic input. Nat. Rev. Neurosci. 1, 181–190.

Maljevic, S., Lerche, H., 2014. Potassium channel genes and benign familial neonatal epilepsy. Prog. Brain Res. 213, 17–53.

Maljevic, S., Wuttke, T.V., Lerche, H., 2008. Nervous system KV7 disorders: breakdown of a subthreshold brake. J. Physiol. 586, 1791–1801.

Miceli, F., Soldovieri, M.V., Ambrosino, P., Ambrosino, P., Barrese, V., Migliore, M., Cilio, M.R., Tagalialatela, M., 2013. Genotype–phenotype correlations in neonatal epilepsies caused by mutations in the voltage sensor of K(v)7.2 potassium channel subunits. Proc. Natl. Acad. Sci. U. S. A. 110, 4386–4391.

Miceli, F., Soldovieri, M.V., Ambrosino, P., De Maria, M., Migliore, M., Migliore, R., Tagalialatela, M., 2015. Early-onset epeilptic encephalopathy caused by gain of function mutations in the voltage sensor of Kv7.2 and Kv7.3 potassium channel subunits. J. Neurosci. 35, 3782–3793.

Milh, M., Boutry-Kryza, N., Sutera-Sardo, J., Mignot, C., Auvin, S., Lacoste, C., Villeneuve, N., Roubertie, A., Heron, B., Carneiro, M., Kaminska, A., Altuzarra, C., et al., 2013. Similar early characteristics but variable neurological outcome of patients with a de novo mutation of KCNQ2. Orphanet J. Rare Dis. 8, 80.

Numis, A.L., Angriman, M., Sullivan, J.E., Lewis, A.J., Striano, P., Nabbout, R., Cilio, M.R., 2014. KCNQ2 encephalopathy: delineation of the electroclinical phenotype and treatment response. Neurology 82, 368–370.

Orhan, G., Bock, M., Schepers, D., Llina, E.I., Reichel, S.N., Löffler, H., Jezutkovic, N., Wechhuysen, S., Mandelstam, S., Danker, T., Guenther, E., Scheffer, I.E., de Jonghe, P., Lerche, H., Maljevic, S., 2014. Dominant-negative effects of KCNQ2 mutations are associated with epileptic encephalopathy. Ann. Neurol. 75, 382–394.

Pan, Z., Kao, T., Horvath, Z., Lemos, J., Sul, J.Y., Cranstoun, S.D., Bennett, V., Scherer, S.S., Cooper, E.C., 2006. A common ankyrin-G-based mechanism retains KCNQ and NaV channels at electrically active domains of the axon. J. Neurosci. 26, 2599–2613.

Peters, H.C., Hu, H., Pongs, O., Storm, J.F., Isbrandt, D., 2005. Conditional transgenic suppression of M channels in mouse brain reveals functions in neuronal excitability, resonance and behavior. Nat. Neurosci. 8, 51–60.

Rasmussen, H.B., Frøkjaer-Jensen, C., Jensen, C.S., Jensen, H.S., Jorgensen, N.K., Misonou, H., Trimmer, J.S., Olesen, S.P., Schmitt, N., 2007. Requirement of subunit co-assembly and ankyrin-G for M-channel localization at the axon initial segment. J. Cell Sci. 120, 953–963.

Safiulina, V.F., Zacchi, P., Tagalialatela, M., Yaari, Y., Cherubini, E., 2008. Low expression of Kv7/M channels facilitates intrinsic and network bursting in the developing rat hippocampus. J. Physiol. 586, 5437–5453.

Shah, M.M., Migliore, M., Valencia, I., Cooper, E.C., Brown, D.A., 2008. Functional significance of axonal Kv7 channels in hippocampal pyramidal neurons. Proc. Natl. Acad. Sci. U. S. A. 105, 7869–7874.

Shah, M.M., Migliore, M., Brown, D.A., 2011. Differential effects of Kv7 (M−) channels on synaptic integration in distinct subcellular compartments of rat hippocampal pyramidal neurons. J. Physiol. 589, 6029–6038.

Singh, N.A., Charlier, C., Stauffer, D., DuPont, B.R., Leach, R.J., Melis, R., Ronen, G.M., Bjerre, I., Quattlebaum, T., Murphy, J.V., McHarg, M.L., Gagnon, D., Rosales, T.O., Peiffer, A., Anderson, V.E., Leppert, M., 1998. A novel potassium channel gene, KCNQ2, is mutated in an inherited epilepsy of newborns. Nat. Genet. 18, 25–29.

Soh, H., Pant, R., LoTurco, J.J., Tzingounis, A.V., 2014. Conditional deletions of epilepsy-associated KCNQ2 and KCNQ3 channels from cerebral cortex cause differential effects on neuronal excitability. J. Neurosci. 34, 5311–5321.

Soldovieri, M.V., Castaldo, P., Iodice, L., Miceli, F., Barrese, V., Bellini, G., Miraglia del Giudice, E., Pascotto, A., Annunziato, L., Tagalialatela, M., 2006. Decreased subunit stability as a novel mechanism for potassium current impairment by a KCNQ2 C terminus mutation causing benign familial neonatal convulsions. J. Biol. Chem. 281, 418–428.

Soldovieri, M.V., Boutry-Kryza, N., Milh, M., Doummar, D., Heron, B., Bourel, E., Ambrosino, P., Miceli, F., De Maria, M., Dorison, N., Auvin, S., Echenne, B., Oertel, J., Riquet, A., Lambert, I., Gerard, M., Roubergue, A., Calender, A., Mignot, C., Tagalialatela, M., Lesca, G., 2014. Novel KCNQ2 and KCNQ3 mutations in a large cohort of families with benign neonatal epilepsy: first evidence for an altered channel regulation by syntaxin 1A. Hum. Mutat. 35, 356–367.

Steinlein, O.K., Conrad, C., Weidner, B., 2007. Benign familial neonatal convulsions: always beningn? Epilepsy Res. 73, 245–249.

Wang, H.S., Pan, Z., Shi, W., Brown, B.S., Wymore, R.S., Cohne, I.S., Dixon, J.E., McKinnon, D., 1998. KCNQ2 and KCNQ3 potassium channel subunits: molecular correlates of the M-channel. Science 282, 1890–1893.

Weckhuysen, S., Mandelstam, S., Suls, A., Audenaert, D., Deconinck, T., Claes, L.R., Deprez, L., Smets, K., Hristova, D., Roelens, F., Lagae, L., Yendle, S., Stanley, T., Heron, S.E., Mulley, J.C., Berkovic, S.F., Scheffer, I.E., De Jonghe, P., 2012. KCNQ2 encephalopathy: emerging phenotype of a neonatal epileptic encephalopathy. Ann. Neurol. 71, 15–25.

Wen, H., Levitan, I.B., 2002. Calmodulin is an auxiliary subunit of KCNQ2/3 potassium channels. J. Neurosci. 22, 7991–8001.

Xiong, Q., Sun, H., Zhang, Y., Nan, F., Li, M., 2008. Combinatorial augmentation of voltage-gated KCNQ potassium channels by chemical openers. Proc. Natl. Acad. Sci. U. S. A. 105, 3128–3133.

Yue, C., Yaari, Y., 2006. Axo-somatic and apical dendritic Kv7/M channels differentially regulate the intrinsic excitability of adult rat CA1 pyramidal cells. J. Neurophysiol. 95, 3480–3495.